Single-Molecule Magnets

International Edition: DOI: 10.1002/anie.201500897
German Edition: DOI: 10.1002/ange.201500897

Redox-Controlled Exchange Bias in a Supramolecular Chain of Fe_4 Single-Molecule Magnets**

*Andrea Nava, Luca Rigamonti, Ennio Zangrando, Roberta Sessoli, Wolfgang Wernsdorfer, and Andrea Cornia**

Abstract: *Tetrairon(III) single-molecule magnets $[Fe_4(pPy)_2(dpm)_6]$ (**1**) (H_3pPy = 2-(hydroxymethyl)-2-(pyridin-4-yl)propane-1,3-diol, Hdpm = dipivaloylmethane) have been deliberately organized into supramolecular chains by reaction with $Ru^{II}Ru^{II}$ or $Ru^{II}Ru^{III}$ paddlewheel complexes. The products $[Fe_4(pPy)_2(dpm)_6][Ru_2(OAc)_4](BF_4)_x$ with $x = 0$ (**2a**) or $x = 1$ (**2b**) differ in the electron count on the paramagnetic diruthenium bridges and display hysteresis loops of substantially different shape. Owing to their large easy-plane anisotropy, the $s = 1$ diruthenium(II,II) units in **2a** act as effective $s_{eff} = 0$ spins and lead to negligible intrachain communication. By contrast, the mixed-valent bridges ($s = 3/2$, $s_{eff} = 1/2$) in **2b** introduce a significant exchange bias, with concomitant enhancement of the remnant magnetization. Our results suggest the possibility to use electron transfer to tune intermolecular communication in redox-responsive arrays of SMMs.*

Single-molecule magnets (SMMs) provide nanoscale, chemically tuneable units displaying magnetic hysteresis and quantum magnetism at the molecular level.[1] Their magnetic moment is amenable to be probed and controlled by electric currents or electromagnetic radiation; consequently, SMMs have been proposed as components for molecular spintronic devices[2] or as qubits for quantum computation.[3,4] To this aim, molecules need to be stably interfaced with the environment while preserving their properties.[5] Additionally, weak coupling between two or more SMMs can be used to further enhance their functionality. First, each SMM can act as a bias on its neighbor(s), generating a better memory effect. Second, entanglement between quantum states is an important resource for quantum information processing.[4] Supramolecular C−H···Cl hydrogen-bonded pairs of Mn_4 complexes (S = 9/2) demonstrated such coupling for the first time.[6] Since then, more supramolecular dimers,[7] chains,[8] and 3D networks[9] have been described in which SMMs interact weakly through hydrogen bonds or other short contacts. Anyway, such supramolecular organizations are largely serendipitous in nature and are disrupted upon dissolution. Alternative approaches to exchange-biased SMM aggregates were proposed by the research groups of Clérac, Christou, and Hendrickson based on coordination bonds;[10–12] general strategies to controlled association of SMMs into coordination networks have been reviewed by Clérac et al.[13]

We herein describe the fully controlled assembly of a tetrairon(III) SMM[14] with an $S = 5$ ground state, $[Fe_4(pPy)_2(dpm)_6]$ (**1**), into 1D supramolecular structures held together by coordination bonds. In **1**, Hdpm is dipivaloylmethane and H_3pPy is 2-(hydroxymethyl)-2-(pyridin-4-yl)propane-1,3-diol, a tripodal ligand bearing a 4-pyridyl substituent. This SMM acts as a ditopic supramolecular synthon and reacts with paddlewheel dimers $[Ru_2(OAc)_4(MeOH)_2]$[15] and $[Ru_2(OAc)_4(THF)_2](BF_4)$[16] to give supramolecular chains $[Fe_4(pPy)_2(dpm)_6][Ru_2(OAc)_4](BF_4)_x$ with $x = 0$ (**2a**) or 1 (**2b**), respectively (OAc = acetate and THF = tetrahydrofuran). The mixed-valent paddlewheel and some isostructural 3d metal dimers were previously used to link Cr_7Ni rings[17] but not SMMs. Both bridging diruthenium units are paramagnetic with $s = 1$ and 3/2, respectively. However, because of their large easy-plane anisotropy normal to the chain direction, at low temperature they act as effective spins with $s_{eff} = 0$ and 1/2, respectively. By consequence, the two compounds greatly differ in intrachain communication, showing that intermolecular magnetic interactions in these systems are amenable to redox control (Figure 1).

Compound **1** was assembled by reaction of the dimer $[Fe_2(OEt)_2(dpm)_4]$ with $FeCl_3$ in the presence of excess tripodal ligand H_3pPy and piperidine as a base in ethanol–diethyl ether solution. It was isolated as X-ray quality crystals of **1**·2 EtOH by vapor diffusion of ethanol into the reaction

[*] A. Nava, Dr. L. Rigamonti, Prof. A. Cornia
Dipartimento di Scienze Chimiche e Geologiche
Università di Modena e Reggio Emilia &
INSTM RU of Modena and Reggio Emilia
via G. Campi 183, 41125 Modena (Italy)
E-mail: acornia@unimore.it
Homepage: http://www.corniagroup.unimore.it
A. Nava
Dipartimento di Scienze Fisiche
Informatiche e Matematiche
Università di Modena e Reggio Emilia, 41125 Modena (Italy)
Prof. E. Zangrando
Dipartimento di Scienze Chimiche e Farmaceutiche
Università di Trieste, 34127 Trieste (Italy)
Prof. R. Sessoli
Laboratory of Molecular Magnetism (LAMM)
Dipartimento di Chimica "Ugo Schiff"
Università di Firenze &
INSTM RU of Florence, 50019 Sesto Fiorentino (Italy)
Dr. W. Wernsdorfer
Institut Néel, CNRS, 38042 Grenoble Cedex 9 (France)

[**] We thank the European Research Council and Italian MIUR for funding through the Advanced Grant MolNanoMas (grant number 267746) and a FIRB project (grant number RBAP117RWN), respectively, and Dr. Giordano Poneti (Università di Firenze) for his help with the magnetic measurements.

Supporting information for this article is available on the WWW under http://dx.doi.org/10.1002/anie.201500897.

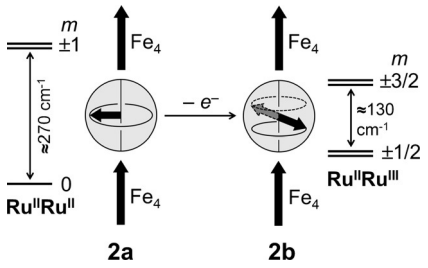

Figure 1. Effect of electron count on the magnetic properties of Ru_2 bridges in **2a** and **2b**. Bold arrows depict spin vectors at Fe_4 and Ru_2 sites. The leftmost and rightmost diagrams show the large zero-field splittings that give rise to a nonmagnetic $m=0$ ground singlet and an $m=\pm1/2$ ground doublet in $Ru^{II}Ru^{II}$ ($s=1$) and $Ru^{II}Ru^{III}$ ($s=3/2$), respectively.

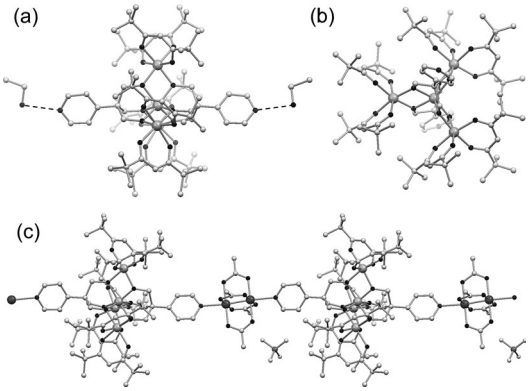

Figure 2. Molecular structure of **1**·2EtOH viewed along the *c* axis (a) and along the *a* axis (b). The side view in (a) includes the hydrogen-bonded ethanol molecules in their highest-occupancy position. c) Structure of **2b** viewed along the *b* axis showing two repeating units running along the *c* axis. Fe = large light gray, Ru = large dark gray, O/N/B = black, C/F = light gray. Hydrogen atoms are omitted for clarity.

mixture. Selected geometrical parameters are reported in Table S1, while the molecular structure is shown in Figure 2.

Slow diffusion of a THF solution of the diruthenium(II,II) complex $[Ru_2(OAc)_4(MeOH)_2]$ into a solution of **1**·2EtOH in CH_2Cl_2 under inert atmosphere afforded **2a** as tiny red crystals, according to Equation (1) ($L=$MeOH, $x=0$).

$$[Fe_4(pPy)_2(dpm)_6]\cdot 2\,EtOH + [Ru_2(OAc)_4(L)_2](BF_4)_x \rightarrow [Fe_4(pPy)_2(dpm)_6][Ru_2(OAc)_4](BF_4)_x\ (\mathbf{2a},\mathbf{b}) + 2\,L + 2\,EtOH \quad (1)$$

Crystals of **2a** are exceedingly air-sensitive and very weak X-ray diffractors even with synchrotron radiation. A preliminary, low-quality data collection revealed the position of all non-hydrogen atoms and confirmed a polymeric structure with $Fe^c\cdots Ru$ distances of 9.3 Å and markedly nonlinear geometry (in the following, Fe^c and Fe^p will indicate central and peripheral iron ions, respectively). The asymmetric unit contains one tetrairon(III) and one diruthenium(II) complex, with a 43.9° angle between Fe_4 and RuO_4 planes (Figure S1 in the Supporting Information).

Reaction of **1**·2EtOH with the mixed-valent complex $[Ru_2(OAc)_4(THF)_2](BF_4)$ in THF, followed by vapour diffusion of toluene under inert atmosphere, afforded the polymeric chain **2b** in good yield as tiny red-brown rods [see Eq. (1) with $L=$THF, $x=1$]. Crystals of **2b** are air-stable but only suitable for X-ray diffraction experiments using synchrotron radiation. The compound crystallizes in the monoclinic space group *Pn* with two tetrairon(III) SMMs, two diruthenium complexes, and two BF_4^- anions in the asymmetric unit. The pyridyl nitrogen atoms of Fe_4 complexes coordinate the ruthenium atoms in the apical position replacing THF molecules, and generating two crystallographically independent 1D chains that run along the *c* axis (Figure 2 and Figure S2). Selected geometrical parameters, reported in Table S1, show that the two chains are structurally very similar, as are the Fe_4 units in **2b** and **1**·2EtOH. For example, the $Fe^c\cdots Fe^p$ distances are all in the 3.08–3.13 Å range. The pitch of the propeller-like Fe_4O_6 cores, evaluated as the average dihedral angle between the $Fe^c(O)_2Fe^p$ and Fe_4 planes is 68.7° in **1**·2EtOH and 70.1° in **2b**, hence typical of Fe_4 complexes with tripodal ligands.[14] The $Fe^c\cdots Ru$ separations are all very similar (average = 9.6 Å) and the intrachain $Fe^c\cdots Fe^c$ distance is 21.3 Å. Neighboring chains are closely packed, with BF_4^- anions occupying the cavities in between them (Figure S2); the shortest interchain $Fe^c\cdots Fe^c$ distance is 13.4 Å, while the minimum Fe···Fe separation is 9.9 Å. The two crystallographically-independent Fe_4 molecules are almost coplanar (5.4°) while the dihedral angle between Fe_4 and RuO_4 planes ranges from 23.8 to 25.3° (average = 24.5°).

Similarities between the structures of **2a** and **2b** emerged clearly from their IR absorption bands and matrix-assisted laser desorption/ionization time-of-flight (MALDI-TOF) mass spectra. In both compounds, the C=O and C=N stretching bands of dpm^- and pPy^{3-} ligands (1500–1600 cm^{-1}) change their relative intensities as compared with **1** and signals due to acetato ligands appear at 1433 and 692 cm^{-1} in **2a** and at 1444 and 691 cm^{-1} in **2b**; the latter also shows a BF_4^- band at 1084 cm^{-1}, which is absent in **2a** (Figure S3). The positive-ion MALDI-TOF mass spectra of **2a** and **2b** display an isotopic cluster of the diad $[Fe_4(pPy)_2(dpm)_6][Ru_2(OAc)_4]^+$ centered at $m/z=2122.5$ (Figure S4 and Table S2).

The temperature dependence of the low field (1–10 kOe) molar magnetic susceptibility (χ_M) for **1**·2EtOH, **2a**, and **2b** was measured between 1.9 and 300 K along with field-dependent isothermal molar magnetization (M_M) data at 4.5, 2.5, and 1.9 K. The $\chi_M T$-vs-T and M_M-vs-H/T curves, reported in Figure S5, are typical of Fe_4 systems,[14] with **2b** significantly more magnetic than the other two compounds because of the presence of the $s=3/2$ Ru_2 unit.[18] Since Fe_4-Ru_2 magnetic interactions are expected to cover a much smaller energy scale than intramolecular Fe-Fe couplings and magnetic anisotropies, we assumed independent Fe_4 and Ru_2 units and subtracted the expected Ru_2 contribution from the data using typical *g*-values and zero-field splitting (zfs) parameters (D') for $Ru^{II}Ru^{II}$ ($s=1$, $g_{Ru}=2.15$, $D'=270\ cm^{-1}$)[18,19] and $Ru^{II}Ru^{III}$ ($s=3/2$, $g_{Ru}=2.08$, $D'=63\ cm^{-1}$).[18,20] The resulting data were satisfactorily reproduced by Heisenberg (for $\chi_M T$-vs-T) or axial zfs (for M_M-vs-H) Hamiltonians with parameters typical for Fe_4 SMMs (see the Supporting Information).[14]

The magnetization dynamics of **1**·2 EtOH, **2a**, and **2b** was then investigated by alternating current (ac) susceptibility measurements at temperatures above 1.8 K and in both zero and 1 kOe applied static field. This H value was found effective in minimizing relaxation by quantum tunnelling (QT; Figure S6). In all cases a temperature dependence of the maxima in the χ_M''-vs-ν plots was observed (Figure S6), demonstrating that the three compounds behave as SMMs. Within the Debye model[21] commonly employed to analyze ac response, a maximum in χ_M'' is observed when the relaxation time τ equals $(2\pi\nu)^{-1}$. The linear $\ln(\tau)$-vs-$1/T$ dependence in the Arrhenius plots of Figure 3 indicates

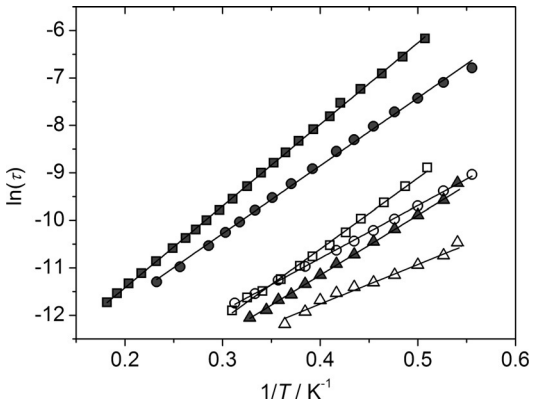

Figure 3. Arrhenius plots for compounds **1**·2 EtOH (□), **2a** (○), and **2b** (△) obtained from alternating current susceptibility measurements in zero (empty symbols) and 1 kOe (full symbols) applied static fields.

thermally activated relaxation in the explored temperature range (see Table S3 for best-fit parameters). Significantly, while Fe_4 units display similar zfs D values in the three compounds, the anisotropy barriers U_{eff}/k_B follow the trend **2b** (12.63(7) K) < **2a** (14.30(17) K) < **1**·2 EtOH (17.20(7) K) at 1 kOe, indicating that both $Ru^{II}Ru^{II}$ and $Ru^{II}Ru^{III}$ bridges enhance underbarrier relaxation over isolated Fe_4 units. The greater effect of $Ru^{II}Ru^{III}$ is explained by the $m = \pm 1/2$ doublet stabilized by the large positive zfs, as opposed to the $m = 0$ singlet of $Ru^{II}Ru^{II}$ (in the following, the Fe_4 and Ru_2 spin substates will be labelled by M and m quantum numbers, respectively). The two complexes then behave as effective $s_{eff} = 1/2$ and 0, respectively (Figure 1), and fast fluctuations of the former may provide a source of QT (see below). Zero-field ac measurements show shorter τ values and lower barriers but a similar trend in the three compounds. All measurements indicate a narrow distribution of relaxation times, with in-field α values[21] ranging from 0.13 to 0.17 at 1.9 K (see the Supporting Information).

To probe the electronic structure over a much smaller energy scale, magnetic hysteresis loops were recorded on single crystals of **1**·2 EtOH, **2a**, and **2b** using a microSQUID apparatus and applying the magnetic field along the easy axis. In all cases, coercivity was found to increase with decreasing temperature and increasing scan rate, as expected for SMM behavior. Measurements on **1**·2 EtOH showed that QT-driven relaxation is reached below 0.3 K. Faster relaxation because of resonant QT of individual Fe_4 centers leads to steps in the hysteresis loops at regular field intervals of $|D|/(g\mu_B) \approx 0.5$ T (see Figures S7 and S8), with pre-step features typical of spin-spin cross relaxation promoted by intermolecular dipole-dipole interactions.[22] Dipolar interactions through the lattice also shift the "zero-field" QT resonance slightly to positive fields (about 10 mT), in accordance with previous findings;[22] such relaxation process around zero field remains visible even at the lowest temperature (0.03 K) and with the fastest scan rate (0.280 T s^{-1}).

The hysteresis loops of **2a** (Figure 4 and Figures S9 and S10) closely resemble those of **1**·2EtOH. Magnetization steps

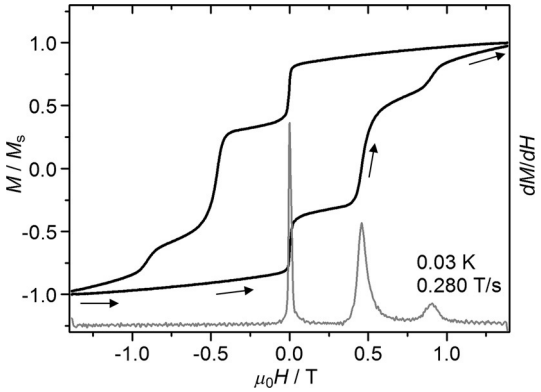

Figure 4. Magnetic hysteresis loop recorded on a single crystal of **2a** along with dM/dH curve (gray). M_s is saturation magnetization.

are detected at 0.00, 0.46, and 0.90 T, in agreement with the behavior of isolated Fe_4 units. The absence of intrachain communication is again explained by considering the integer spin and large positive zfs of the $Ru^{II}Ru^{II}$ complex, which result in a nonmagnetic $m = 0$ ground state (Figure 1).

The behavior of **2b** is remarkably different (Figure 5 a and Figures S11 and S12). At 0.03 K coercivity is reduced as compared with **1**·2 EtOH but a large remnant magnetization, amounting to about 79 % of saturation magnetization (M_s), is found in zero field at all sweep rates explored. Saturation is reached in applied fields larger than about 1 T following a broad, quasi-reversible step at $\pm 0.84(1)$ T. Such enhanced memory effect originates from a pronounced shift of the "zero-field" resonance to ± 0.124 T. A second, pronounced magnetization step is detected between 0.37 and 0.54 T (Figure 5 a), that is, close to the field ($|D|/(g\mu_B)$) where the $M = +5$ to -4 transition typically occurs in isolated Fe_4 complexes.[22] Since dipolar fields within a chain and between chains would not exceed a few millitesla in both **2a** and **2b**, the observed differences in magnetic behavior must arise from superexchange interactions with the Ru_2 units rather than from crystal packing effects.

Neglecting interchain interactions, the behavior of **2b** can be described by a chain model of alternating anisotropic $S = 5$ and $s = 3/2$ spins weakly coupled via Heisenberg exchange. However, as detailed in the Supporting Information, the low-lying spin levels are accurately reproduced by an Ising-like model where only spin components along the Fe_4 easy axis are relevant [Eq. (2)].

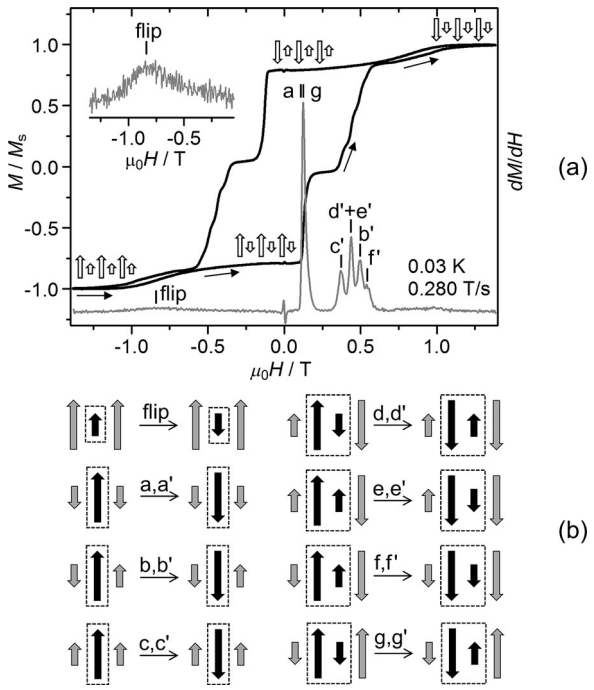

Figure 5. a) Magnetic hysteresis loop recorded on a single crystal of **2b**, along with *dM*/*dH* curve (gray). M_s is saturation magnetization. Vertical ticks mark the spin-flip transition and QT resonances. The derivative signal at $H=0$ is an instrumental artifact. b) Proposed assignment of the steps in the hysteresis loop, with spins rotated by 90° from the chain direction for a simpler representation. Spins undergoing reversal are drawn in black and highlighted by a dashed rectangle, while spins in gray remain fixed. Unprimed and primed letters denote $M=+5\rightarrow-5$ and $M=+5\rightarrow-4$, resonances, respectively.

$$E = D\,\Sigma_i M_{2i}{}^2 + \Sigma_i J_{|M|} M_{2i}(m_{2i-1} + m_{2i+1}) + \mu_B B\,\Sigma_i\,(g M_{2i} + g_{\mathrm{eff}}\, m_{2i-1}) \quad (2)$$

The first term accounts for magnetic anisotropy at Fe_4 centers that are located on even-*i* sites. The Ru_2 complexes occupy odd-*i* sites and, owing to their large easy-plane anisotropy, are described by $m=\pm 1/2$ and an anisotropic *g*-factor $g_{\mathrm{eff}}=(g_{\parallel}{}^2\cos^2\theta + g_{\perp}{}^2\sin^2\theta)^{1/2}$, with $g_{\parallel}=g_{\mathrm{Ru}}$ and $g_{\perp}=2g_{\mathrm{Ru}}$.[23] Here, θ is the angle between the Fe_4 and Ru_2 anisotropy axes ($\theta\approx 25°$ from crystal structure, whence $g_{\mathrm{eff}}\approx 2.60$). $J_{|M|}$ is the effective Fe_4-Ru_2 exchange-coupling constant, which can be different when the Fe_4 complex occupies the $M=\pm 5$ or the $M=\pm 4$ doublet (see the Supporting Information). Differences with the electronic structure of **2a** are pictured in Figure 1.

We now analyze the field dependence of the magnetization in terms of the most probable tunnelling events, that is, individual or pairwise spin reversals, following the pathway marked by arrows in Figure 5a. The application of a large negative ("down") field aligns all the spins in the upward direction, that is, $M=+5$ and $m=+1/2$ at all sites. As the field magnitude declines, the broad step detected at $-0.84(1)$ T is suggestive of antiferromagnetic Fe_4-Ru_2 coupling and of a spin-flip transition, whereby all Ru_2 spins reverse to $m=-1/2$. At the transition field, the decrease in exchange energy exactly equals the increase in Zeeman energy, that is, $|B_{\mathrm{flip}}|=10J_5/(g_{\mathrm{eff}}\mu_B)$, whence $J_5\approx 0.10\ \mathrm{cm}^{-1}$ for $g_{\mathrm{eff}}\approx 2.60$. By consequence an effective ferromagnetic coupling is established between Fe_4 units, a rare situation in supramolecular SMM assemblies.[9f,24] This coupling strength confirms that in the temperature range explored by ac susceptibility measurements the condition $k_B T > 10J_5$ holds and substantial fluctuations of $Ru^{II}Ru^{III}$ spins are to be expected. After the spin-flip transition, the magnetization remains virtually constant up to about 0.10 T and no zero-field QT resonance is detected. In fact, for a resonant tunnelling event to occur the initial and final states must have the same energy, that is, the decrease in Zeeman energy upon QT must exactly compensate the increase in exchange and anisotropy energies. It is straightforward to show that, for a given Fe_4 center in the chain, the QT transitions from $M=+5$ to -5 and from $M=+5$ to -4 are split into three depending on the $m_{\mathrm{L(R)}}$ value of its lefthand L (righthand R) Ru_2 neighbors. In much the same way, a ^{1}H nucleus coupled to two equivalent neighbors gives a triplet in NMR spectra. The two groups of resonances (a,b,c and a′,b′,c′ in Figure 5b), should occur at fields [Eqs. (3) and (4)]

$$B = -J_5(m_L + m_R)/(g\mu_B) \quad (3)$$

$$B' = |D|/(g\mu_B) - [(5/9)J_5 + (4/9)J_4](m_L + m_R)/(g\mu_B) \quad (4).$$

Then, the term proportional to $m_L + m_R$ may be conveniently viewed as "bias field" that adds to the external field and shifts the resonances. Because after the spin-flip transition all Fe_4 spins are "up" ($M=+5$) and all Ru_2 spins are "down" ($m=-1/2$), relaxation around zero field may only start through a QT resonance involving this initial state (resonance a in our scheme). Setting $J_5=0.10\ \mathrm{cm}^{-1}$ and $m_L=m_R=-1/2$ in Equation (3) one finds $B=0.11$ T, in reasonable agreement with the sharp increase of the magnetization at 0.124 T. The further increase of the magnetization between 0.37 and 0.54 T occurs in four substeps at 0.374, 0.439, 0.494, and 0.545 T, as most clearly shown by the first-derivative curve in Figure 5a. The spacing between the first and third substeps (0.120 T) is virtually identical to the bias field that affects the "zero-field" resonance, suggesting that exchange energy may be at the origin of the observed fine structure. When the first and third substeps are assigned to resonances c′ and b′ [i.e. $m_L+m_R=1$ and 0 in Eq. (4)], it follows that $D=-0.46\ \mathrm{cm}^{-1}$, a realistic value for Fe_4 complexes. With this assignment, resonance a′ would occur at 0.61 T, that is, in a field region where "up" Fe_4 spins are no longer available. Notice that approximately half of the Fe_4 spins have already reversed at around 0.2–0.3 T, so that $m_L=m_R=-1/2$ is by no means the only accessible initial state. The two remaining substeps are not accounted for by the exchange-biased flipping of individual Fe_4 spins, but can be explained by the simultaneous reversal of a Fe_4 spin and a neighboring Ru_2 unit. Considering the spin arrangement within the pair and the orientation of the two adjacent spins, eight different QT events of this type can be envisaged, the resonant fields of which are easily worked out from Equation (2) (see the Supporting Information). Among them, three resonances are indeed predicted at 0.452 (d′), 0.431 (e′), and 0.525 T (f′), hence close to the second and fourth substeps (see Figure 5b). In addition, resonance g is expected at

0.123 T and can also contribute to the relaxation step around zero field, for it has the same initial state as resonance a. With this assignment, all step positions are reproduced within 4 mT using the following set of spin Hamiltonian parameters: $g = 2.00$ (fixed), $D = -0.465(2)\ cm^{-1}$, $J_5 = 0.101(1)\ cm^{-1}$, $J_4 = 0.133(7)\ cm^{-1}$ and $g_{eff} = 2.57(4)$. The best-fit g_{eff} value is fully consistent with the typical Landè factor of diruthenium(II,III) paddlewheels[18,20] and with the θ value estimated from the crystal structure. Moreover, the relative magnetization change at the spin-flip transition $(5g - g_{eff}/2)/(5g + g_{eff}/2) = 0.77$ is in good agreement with the measured value (0.79). All experimental features are thus reproduced with great accuracy by our relatively simple model, confirming that Fe_4 complexes are an ideal work bench for investigating quantum effects in the dynamics of the magnetization.

In conclusion, we have harnessed the chemical versatility of Fe_4 complexes to prepare chain-like assemblies of SMM units bridged by diruthenium paddlewheels in two different oxidation states. The diruthenium(II,II) bridges in **2a** have $s = 1$, but their large easy-plane anisotropy results in a non-magnetic $m = 0$ ground singlet and in negligible intrachain communication. By contrast, the diruthenium(II,III) bridges have half-integer ($s = 3/2$) spin but maintain a large easy-plane anisotropy. By virtue of their $m = \pm 1/2$ ground doublet, they act as effective magnetic couplers and compound **2b** behaves as a significantly better magnet in zero field than an array of non-interacting Fe_4 centers. While redox-controllable SMM cores are a topic of great current interest,[25] the new behavior herein described suggests the possibility to prepare redox-responsive arrays of SMMs in which intrachain coupling and remnant magnetization are reversibly tuned by electron transfer.

Experimental Section

General procedures: For the preparation of **1**·2 EtOH, other synthetic details, crystal structure determinations and magnetic measurements see the Supporting Information. Compounds **2a** and **2b** were synthesized under inert atmosphere in a drybox and using anhydrous solvents.

2a: A light brown solution of $[Ru_2(OAc)_4(MeOH)_2]$ (50 mg, 0.099 mmol) in THF (20 mL) was layered over a red solution of compound **1**·2 EtOH (168 mg, 0.0946 mmol) in CH_2Cl_2 (20 mL) with a 2 mL CH_2Cl_2 buffer. The tiny red crystals formed after ten days were collected by filtration, washed with *n*-hexane and dried (129 mg, 64.2 %). The compound maintains its crystallinity when stored in its mother liquor or covered with vacuum grease. Elemental analysis (%) calcd for $C_{92}H_{146}Fe_4N_2O_{26}Ru_2$ (2121.66): C 52.08, H 6.94, N 1.32; found for dried sample: C 51.79, H 7.05, N 1.40; IR (KBr): $\tilde{\nu}$ =2963 (s; ν(C-H_{tBu})), 1592 (s), 1576 (vs), 1564 (vs), 1549 (vs), 1505 (vs; ν(C=O_{dpm}, C=N_{pPy})), 1433 (s; ν(C=O_{AcO})), 1401 (s), 1385 (s), 1357 (s; ν(CH_3)), 1106 (m; ν(C-O_{pPy})), 692 (w; δ(AcO)), 562 cm^{-1} (m; δ(py)). MALDI-TOF (THF): *m/z* (%): 2122.52 (5) [M^+], 1721.58 (1) [$Fe_4(pPy)_2(dpm)_6 + K^+$], 1705.61 (2) [$Fe_4(pPy)_2(dpm)_6 + Na^+$], 1499.49 (30) [$Fe_4(pPy)_2(dpm)_5^+$], 1316.34 (90) [$Fe_4(pPy)_2(dpm)_4^+$], 439.79 (40) [$Ru_2(OAc)_4^+$], 422.16 (100) [$Fe(dpm)_2^+$].

2b: Compound **1**·2 EtOH (101 mg, 0.0569 mmol) and [$Ru_2(OAc)_4(THF)_2$](BF_4) (40 mg, 0.060 mmol) were dissolved in THF (20 and 12 mL, respectively) and mixed together. Slow vapor diffusion of toluene (42 mL) gave the title compound as tiny red-brown crystals, which were extensively washed with CH_2Cl_2 until colorless washings (97.5 mg, 77.6 %). Elemental analysis (%) calcd for $C_{92}H_{146}BF_4Fe_4N_2O_{26}Ru_2$ (2208.47): C 50.03, H 6.66, N 1.27; found: C 49.69, H 6.92, N 1.41. IR (KBr): $\tilde{\nu}$ =2964 (s; ν(C-H_{tBu})), 1592 (s), 1576 (vs), 1564 (vs), 1549 (vs), 1538 (vs), 1505 (vs; ν(C=O_{dpm}, C=N_{pPy})), 1444 (s; ν(C=O_{AcO})), 1401 (s), 1385 (s), 1357 (s; ν(CH_3)), 1107 (m; ν(C-O_{pPy})), 1084 (m; ν(BF_4)), 691 (m; δ(AcO)), 564 cm^{-1} (m; δ(py)). MALDI-TOF (THF): *m/z* (%): 2122.41 (5) [$M - BF_4^-$], 1705.57 (1) [$Fe_4(pPy)_2(dpm)_6 + Na^+$], 1499.40 (20) [$Fe_4(pPy)_2(dpm)_5^+$], 1316.28 (30) [$Fe_4(pPy)_2(dpm)_4^+$], 439.79 (40) [$Ru_2(OAc)_4^+$], 422.15 (100) [$Fe(dpm)_2^+$].

Keywords: chain structures · iron · magnetic properties · ruthenium · single-molecule magnets

How to cite: *Angew. Chem. Int. Ed.* **2015**, *54*, 8777–8782
Angew. Chem. **2015**, *127*, 8901–8906

[1] D. Gatteschi, R. Sessoli, J. Villain, *Molecular Nanomagnets*, Oxford University Press, Oxford, **2006**.
[2] a) S. Thiele, F. Balestro, R. Ballou, S. Klyatskaya, M. Ruben, W. Wernsdorfer, *Science* **2014**, *344*, 1135–1138; b) R. Vincent, S. Klyatskaya, M. Ruben, W. Wernsdorfer, F. Balestro, *Nature* **2012**, *488*, 357–360.
[3] M. N. Leuenberger, D. Loss, *Nature* **2001**, *410*, 789–793.
[4] a) F. Troiani, M. Affronte, *Chem. Soc. Rev.* **2011**, *40*, 3119–3129; b) C. J. Wedge, G. A. Timco, E. T. Spielberg, R. E. George, F. Tuna, S. Rigby, E. J. L. McInnes, R. E. P. Winpenny, S. J. Blundell, A. Ardavan, *Phys. Rev. Lett.* **2012**, *108*, 107204.
[5] A. Cornia, M. Mannini, *Struct. Bonding (Berlin)* **2015**, *164*, 293–330.
[6] a) W. Wernsdorfer, N. Aliaga-Alcalde, D. N. Hendrickson, G. Christou, *Nature* **2002**, *416*, 406–409; b) S. Hill, R. S. Edwards, N. Aliaga-Alcalde, G. Christou, *Science* **2003**, *302*, 1015–1018; c) R. Tiron, W. Wernsdorfer, D. Foguet-Albiol, N. Aliaga-Alcalde, G. Christou, *Phys. Rev. Lett.* **2003**, *91*, 227203.
[7] R. Bagai, W. Wernsdorfer, K. A. Abboud, G. Christou, *J. Am. Chem. Soc.* **2007**, *129*, 12918–12919.
[8] L. Lecren, W. Wernsdorfer, W.-G. Li, A. Vindigni, H. Miyasaka, R. Clérac, *J. Am. Chem. Soc.* **2007**, *129*, 5045–5051.
[9] a) R. Tiron, W. Wernsdorfer, N. Aliaga-Alcalde, G. Christou, *Phys. Rev. B* 2003, 68, 140407; b) E.-C. Yang, W. Wernsdorfer, S. Hill, R. S. Edwards, M. Nakano, S. Maccagnano, L. N. Zakharov, A. L. Rheingold, G. Christou, D. N. Hendrickson, *Polyhedron* 2003, 22, 1727–1733; c) E.-C. Yang, W. Wernsdorfer, L. N. Zakharov, Y. Karaki, A. Yamaguchi, R. M. Isidro, G.-D. Lu, S. A. Wilson, A. L. Rheingold, Hi. Ishimoto, D. N. Hendrickson, *Inorg. Chem.* 2006, 45, 529–546; d) R. Inglis, L. F. Jones, K. Mason, A. Collins, S. A. Moggach, S. Parsons, S. P. Perlepes, W. Wernsdorfer, E. K. Brechin, *Chem. Eur. J.* 2008, 14, 9117–9121; e) R. Inglis, S. M. Taylor, L. F. Jones, G. S. Papaefstathiou, S. P. Perlepes, S. Datta, S. Hill, W. Wernsdorfer, E. K. Brechin, *Dalton Trans.* 2009, 9157–9168; f) A. Das, K. Gieb, Y. Krupskaya, S. Demeshko, S. Dechert, R. Klingeler, V. Kataev, B. Buchner, P. Müller, F. J. Meyer, *J. Am. Chem. Soc.* 2011, 133, 3433–3443.
[10] T. N. Nguyen, W. Wernsdorfer, K. A. Abboud, G. Christou, *J. Am. Chem. Soc.* **2011**, *133*, 20688–20691.
[11] J. Yoo, W. Wernsdorfer, E.-C. Yang, M. Nakano, A. L. Rheingold, D. N. Hendrickson, *Inorg. Chem.* **2005**, *44*, 3377–3379.
[12] a) L. Lecren, O. Roubeau, Y.-G. Li, X. F. Le Goff, H. Miyasaka, F. Richard, W. Wernsdorfer, C. Coulon, R. Clérac, *Dalton Trans.* **2008**, 755–766; b) L. Lecren, O. Roubeau, C. Coulon, Y.-G. Li, X. F. Le Goff, W. Wernsdorfer, H. Miyasaka, R. Clérac, *J. Am. Chem. Soc.* **2005**, *127*, 17353–17363.
[13] a) I.-E. Jeon, R. Clérac, *Dalton Trans.* **2012**, *41*, 9569–9586; b) O. Roubeau, R. Clérac, *Eur. J. Inorg. Chem.* **2008**, 4325–4342.
[14] a) S. Accorsi, A.-L. Barra, A. Caneschi, G. Chastanet, A. Cornia, A. C. Fabretti, D. Gatteschi, C. Mortalò, E. Olivieri, F. Parenti, P. Rosa, R. Sessoli, L. Sorace, W. Wernsdorfer, L. Zobbi, *J. Am.*

Chem. Soc. **2006**, *128*, 4742 – 4755; b) L. Gregoli, C. Danieli, A.-L. Barra, P. Neugebauer, G. Pellegrino, G. Poneti, R. Sessoli, A. Cornia, *Chem. Eur. J.* **2009**, *15*, 6456 – 6467.

[15] M. C. Barral, R. González-Prieto, R. Jiménez-Aparicio, J. L. Priego, M. R. Torres, F. A. Urbanos, *Inorg. Chim. Acta* **2005**, *358*, 217 – 221.

[16] F. A. Urbanos, M. C. Barral, R. Jiménez-Aparicio, *Polyhedron* **1988**, *7*, 2597 – 2600.

[17] a) M. Affronte, I. Casson, M. Evangelisti, A. Candini, S. Carretta, C. A. Muryn, S. J. Teat, G. A. Timco, W. Wernsdorfer, R. E. P. Winpenny, *Angew. Chem. Int. Ed.* **2005**, *44*, 6496 – 6500; *Angew. Chem.* **2005**, *117*, 6654 – 6658; b) M. Affronte, F. Troiani, A. Ghirri, S. Carretta, P. Santini, V. Corradini, R. Schuecker, C. Muryn, G. Timco, R. E. P. Winpenny, *Dalton Trans.* **2006**, 2810 – 2817; c) G. A. Timco, S. Carretta, F. Troiani, F. Tuna, R. J. Pritchard, C. A. Muryn, E. J. L. McInnes, A. Ghirri, A. Candini, P. Santini, G. Amoretti, M. Affronte, R. E. P. Winpenny, *Nat. Nanotechnol.* **2009**, *4*, 173 – 178; d) G. F. S. Whitehead, B. Cross, L. Carthy, V. A. Milway, H. Rath, A. Fernandez, S. L. Heath, C. A. Muryn, R. G. Pritchard, S. J. Teat, G. A. Timco, R. E. P. Winpenny, *Chem. Commun.* **2013**, *49*, 7195 – 7197.

[18] a) M. A. S. Aquino, *Coord. Chem. Rev.* **1998**, *170*, 141 – 202; b) M. Mikuriya, D. Yoshioka, M. Handa, *Coord. Chem. Rev.* **2006**, *250*, 2194 – 2211.

[19] M. Handa, D. Yoshioka, M. Mikuriya, I. Hiromitsu, K. Kasuga, *Mol. Cryst. Liq. Cryst.* **2002**, *376*, 257 – 262.

[20] a) F. D. Cukiernik, A.-M. Giroud-Godquin, P. Maldivi, J.-C. Marchon, *Inorg. Chim. Acta* **1994**, *215*, 203 – 207; b) E. J. Beck, K. D. Drysdale, L. K. Thompson, L. Li, C. A. Murphy, M. A. S. Aquino, *Inorg. Chim. Acta* **1998**, *279*, 121 – 125.

[21] a) K. S. Cole, R. H. Cole, *J. Chem. Phys.* **1941**, *9*, 341 – 352; b) C. Dekker, A. F. M. Arts, H. W. Wijn, A. J. Van Duyneveldt, J. A. Mydosh, *Phys Rev. B* **1989**, *40*, 11243 – 11251.

[22] L. Vergnani, A.-L. Barra, P. Neugebauer, M. J. Rodriguez-Douton, R. Sessoli, L. Sorace, W. Wernsdorfer, A. Cornia, *Chem. Eur. J.* **2012**, *18*, 3390 – 3398.

[23] R. D. L. Carlin, *Magnetochemistry*, Springer, Berlin, **1986**.

[24] W. Wernsdorfer, S. Bhaduri, A. Vinslava, G. Christou, *Phys. Rev. B* **2005**, *72*, 214429.

[25] a) L. Norel, M. Feng, K. Bernot, T. Roisnel, T. Guizouarn, K. Costuas, S. Rigaut, *Inorg. Chem.* **2014**, *53*, 2361 – 2363; b) S. Fortier, J. J. Le Roy, C.-H. Chen, V. Vieru, M. Murugesu, L. F. Chibotaru, D. J. Mindiola, K. G. Caulton, *J. Am. Chem. Soc.* **2013**, *135*, 14670 – 14678; c) G. N. Newton, S. Yamashita, K. Hasumi, J. Matsuno, N. Yoshida, M. Nihei, T. Shiga, M. Nakano, H. Nojiri, W. Wernsdorfer, H. Oshio, *Angew. Chem. Int. Ed.* **2011**, *50*, 5716 – 5720; *Angew. Chem.* **2011**, *123*, 5834 – 5838.

Received: January 30, 2015
Revised: March 10, 2015
Published online: June 11, 2015

